JMB

Atomic Resolution Structures of CTX-M β-Lactamases: Extended Spectrum Activities from Increased Mobility and Decreased Stability

Yu Chen[1], Julien Delmas[2], Jacques Sirot[2], Brian Shoichet[1]* and Richard Bonnet[1,2]*

[1]*Department of Pharmaceutical Chemistry, University of California, San Francisco Genentech Hall, 600 16th Street San Francisco, CA 94143-2240 USA*

[2]*Laboratoire de Bactériologie Centre Hospitalier Universitaire Faculté de Médecine, 28 Place Henri-Dunant, 63001 Clermont-Ferrand Cedex France*

Extended spectrum β-lactamases (ESBLs) confer bacterial resistance to third-generation cephalosporins, such as cefotaxime and ceftazidime, increasing hospital mortality rates. Whereas these antibiotics are almost impervious to classic β-lactamases, such as TEM-1, ESBLs have one to four orders greater activity against them. The origins of this activity have been widely studied for the TEM and SHV-type ESBLs, but have received less attention for the CTX-M β-lactamases, an emerging family that is now the dominant ESBL in several regions. To understand how CTX-M β-lactamases achieve their remarkable activity, biophysical and structural studies were undertaken. Using reversible, two-state thermal denaturation, it was found that as these enzymes evolve a broader substrate range, they sacrifice stability. Thus, the mutant enzyme CTX-M-16 is eightfold more active against ceftazidime than the pseudo-wild-type CTX-M-14 but is 1.9 kcal/mol less stable. This is consistent with a "stability-activity tradeoff," similar to that observed in the evolution of other resistance enzymes. To investigate the structural basis of enzyme activity and stability, the structures of four CTX-M enzymes were determined by X-ray crystallography. The structures of CTX-M-14, CTX-M-27, CTX-M-9 and CTX-M-16 were determined to 1.10 Å, 1.20 Å, 0.98 Å and 1.74 Å resolution, respectively. The enzyme active sites resemble those of the narrow-spectrum TEM-1 and SHV-1, and not the enlarged sites typical of ESBL mutants such as TEM-52 and TEM-64. Instead, point substitutions leading to specific interactions may be responsible for the improved activity against ceftazidime and cefotaxime, consistent with observations first made for the related Toho-1 enzyme. The broadened substrate range of CTX-M-16 may result from coupled defects in the enzyme's B3 strand, which lines the active site. Substitutions Val231→Ala and Asp240→Gly, which convert CTX-M-14 into CTX-M-16, occur at either end of this strand. These defects appear to increase the mobility of B3 based on anisotropic *B*-factor analyses at ultrahigh resolution, consistent with stability loss and activity gain. The unusually high resolution of these structures that makes such analyses possible also makes them good templates for inhibitor discovery.

© 2005 Elsevier Ltd. All rights reserved.

Keywords: β-lactamase; antibiotic resistance; third generation cephalosporins; X-ray crystallography; enzyme motion

*Corresponding authors

Introduction

The production of β-lactamases is the predominant cause of resistance to β-lactam antibiotics, such as the penicillins and the cephalosporins, in Gram-negative bacteria. β-Lactamases are organized into four classes, designated A to D based on sequence and mechanism. These enzymes cleave the amide

bond in the β-lactam ring, inactivating the anti-biotics. Class A enzymes are most frequently encountered in clinical isolates, often encoded by genes located on transferable plasmids. In the early 1980s, third-generation cephalosporins, such as cefotaxime and ceftazidime, were introduced to treat infections caused by β-lactamase-producing bacteria (Figure 1). These β-lactams have bulky R1 side-chains that make them inherently less
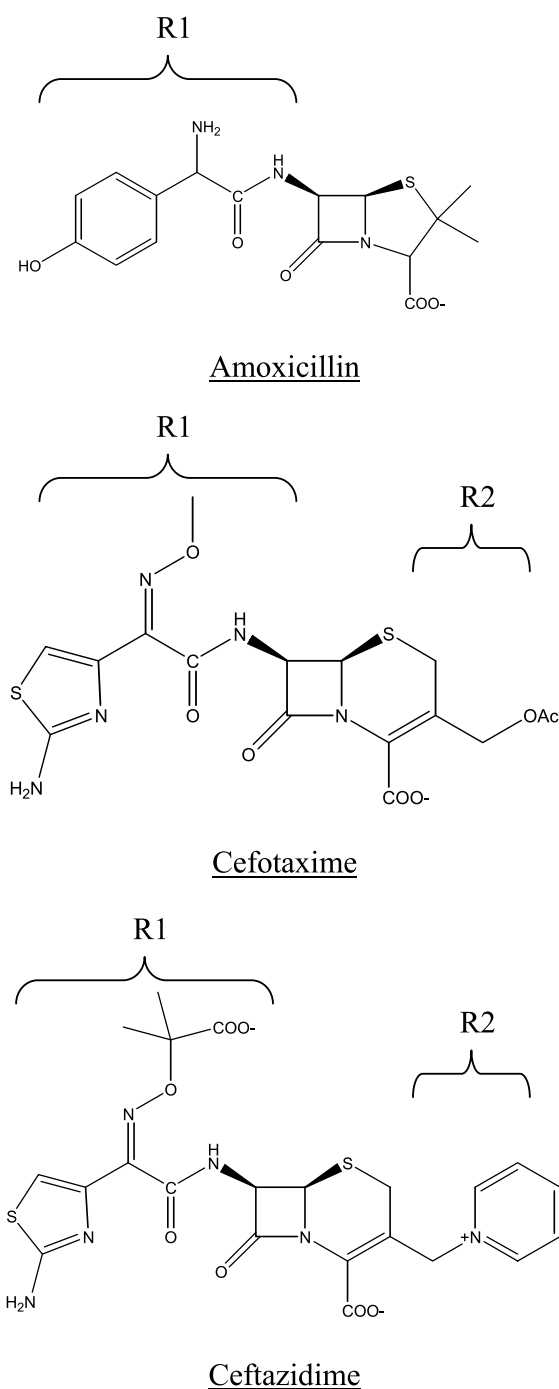

Amoxicillin

Cefotaxime

Ceftazidime

Figure 1. Structures of β-lactam antibiotics: a penicillin (amoxicillin) and two third-generation cephalosporins (cefotaxime and ceftazidime). The R1 and R2 side-chains are labeled.

susceptible to β-lactamases. Unfortunately, their widespread use prompted the emergence of resistant strains that produced class A extended spectrum β-lactamases (ESBLs).[1] This resistance leads to treatment problems in many clinical settings, particularly in intensive care units, significantly increasing mortality.[2]

First observed in 1983, the earliest class A ESBLs involved one to four point mutations in the well-known penicillinases TEM-1 and SHV-1. These substitutions began to extend their hydrolytic spectrum to third-generation cephalosporins; subsequently, over 130 variants of TEM and SHV ESBLs have been described. These enzymes have been the focus of extensive kinetic, modeling, and muta-genesis studies.[3–5] Crystal structures of the enzymes TEM-1,[6–9] TEM-52,[10] TEM(G238A),[4] TEM-64,[4] SHV-1[11] and SHV-2[12] have been reported recently. The structure, activity and stability of these enzymes are now fairly well understood.

Since 1995, a new group of class A ESBLs, the CTX-M enzymes, has been observed worldwide; in some areas these enzymes are now the most frequently observed ESBLs. CTX-M enzymes share less than 40% identity with TEM and SHV-type enzymes and form a relatively heterogeneous family of 40 members, which are sub-classified into five major lineages: CTX-M-1, CTX-M-2, CTX-M-8, CTX-M-9, and CTX-M-25 groups.[13] CTX-M enzymes have a wide substrate range, hydrolyzing the penicillins, the first, second and third-generation cephalosporins (except 7α-methoxy-cephalosporins).

CTX-M enzymes differ from most TEM and SHV ESBLs by a much greater hydrolytic activity against cefotaxime than against ceftazidime and a different susceptibility profile to inhibitors. Also, the activity spectrum among CTX-M enzymes is unusually heterogeneous. The enzyme Toho-1, which belongs to the CTX-M-2 cluster, is more susceptible to inhibition by clavulanate than tazo-bactam (K_i, 0.6 *versus* 5.3 μM),[14] whereas most other CTX-M enzymes exhibit an opposite behavior. Toho-1 has a lower hydrolytic activity against penicillins and higher hydrolytic activity against ceftazidime than the "typical" CTX-M enzymes.[15] Three other atypical CTX-M enzymes have also been reported that exhibit an unusually high level of resistance to ceftazidime. The improved activity *versus* ceftazidime for these three enzymes, CTX-M-15,[16] CTX-M-16[17] and CTX-M-27[18] is correlated with the substitution Asp240Gly, which has never been observed in naturally occurring TEM and SHV-type ESBLs.

Unlike the well studied TEM and SHV β-lactamases, there have been few biophysical or structural studies of the CTX-M family. An important step was the determination of the Toho-1 structure by X-ray crystallography, which significantly advanced our understanding of these enzymes.[15,19,20] A surprising feature of the Toho-1 structure was that its active site resembled that of the narrow spectrum TEM-1 enzyme, and did not

feature the enlarged sites characteristic of ESBL mutants such as TEM-52[10] and TEM-64.[4] In these TEM-derived ESBLs, an increase in active site volume is thought to be key to their ability to recognize the relatively large third generation cephalosporins. Since Toho represents an unusual sub-class of the CTX-M enzymes, it is not clear whether this feature is characteristic of the family. Also, it is uncertain how these enzymes, which take their name from their specialist activity *versus* cefotaxime (CTX), broaden their activity to include ceftazidime, the second most widely used third-generation cephalosporin. Thus, CTX-M-27 and CTX-M-16, which are point mutants of the pseudo-wild-type CTX-M-14 (WT*), are four and eight times more active against ceftazidime than is the WT* enzyme. But how these substitutions increase activity is unclear. In the TEM ESBLs, increased activity came with increased active site volume and decreased enzyme activity, consistent with a "stability-function tradeoff".[21–23] Such a tradeoff has been proposed as characteristic of the evolution of resistance enzymes.[4] If true, it should apply to the CTX-M enzymes. Thus, investigating the structures and biophysics of these enzymes seemed interesting both for particular reasons of understanding and reversing antibiotic resistance, and for understanding basic constraints on the evolution of enzyme activity.

To investigate these questions, we determined the X-ray crystal structures and stability-activity profiles of four CTX-M enzymes. CTX-M-14 and CTX-M-9 are characteristic of the overall family, having extraordinarily high hydrolytic activity against cefotaxime but 1000-fold less activity *versus* ceftazidime. CTX-M-16 and CTX-M-27 are point mutant enzymes that have gained nearly an order of magnitude in activity *versus* ceftazidime.

Comparing the four enzymes allows us to consider general features of the family, as well as substitutions that confer a broader substrate range. To understand if this increased activity occurred at the expense of protein stability, conditions under which the enzymes could be unfolded by reversible, two-state thermal denaturation were developed, and the relative thermodynamic stabilities of the enzymes compared. To investigate the basis of ESBL activity of these enzymes, and those of the stability and activity changes among them, the structures of CTX-M-14, CTX-M-27, CTX-M-9 and CTX-M-16 were determined to 1.10 Å, 1.20 Å, 0.98 Å and 1.74 Å, respectively. These structures reveal aspects of the enzymes in unusual detail, offering insights into the substrate recognition and stability change.

Results

Structure determination

The four enzymes CTX-M-14, CTXM-9, CTX-M-27 and CTX-M-16 were crystallized at pH 4.5 and their structures were determined to high or ultra-high resolution. Consistent with their excellent diffraction, the solvent content of the crystals was relatively low ($\sim$37%). The Toho-1 apo structure (pdb ID, 1IYS) provided the initial phases in molecular replacement. The high quality of the data led to low *R* values after refinement (Table 1).

Overall structure

The backbone structures of the four mutants resemble one another closely, except for small movements at the termini and in loop regions close to the substitution sites. The rmsd value of the

Table 1. Refinement statistics

	CTX-M-14[a]	CTX-M-9[a]	CTX-M-27[a]	CTX-M-16[b]
Resolution (Å)	22–1.10 (1.14–1.10)[c]	22–0.98 (1.02–0.98)	22–1.20 (1.24–1.20)	22–1.74 (1.8–1.74)
Completeness (%)	96.9 (76.4)	95.5 (71.7)	97.3 (93.9)	99.4 (98.5)
R_{merge} (%)[d]	3.7 (27.6)	4.3 (33.6)	5.3 (60.4)	6.2 (36.1)
Unique reflections	89,046 (6916)	122,971 (9128)	69,072 (6566)	23,893 (2307)
$[I]/[\sigma(I)]$	16.2 (2.0)	17.8 (1.8)	13.8 (1.9)	12.1 (2.4)
Space group	$P2_12_12_1$	$P2_12_12_1$	$P2_12_12_1$	$P2_12_12_1$
Unit cell *a, b, c* (Å)	41.5, 62.4, 86.7	41.4, 62.2, 85.7	41.5, 62.8, 86.0	41.5, 62.4, 86.7
Number of residues with double conformations	21	23	19	/
R_{work} (%)	12.4	10.8	13.2	17.3
R_{free} (%)	15.7	13.0	15.8	20.4
rmsd from ideality				
Bond lengths (Å)	0.014	0.017	0.006	0.005[b]
Angle distances (Å)[a]/angles (deg.)[b]	0.031	0.033	0.020	1.31[b]
Ramachandran plot[e]				
Most favored (%)	92.0	89.4	92.0	91.6
Additionally allowed (%)	7.5	9.7	7.1	8.0
Generously allowed (%)	0.4	0.9	0.9	0.4

[a] Refined by SHELXL-97.[42]
[b] Refined by CNS1.1.[43]
[c] Values in parentheses represent the highest resolution shells.
[d] Calculated by SCALEPACK.[41]
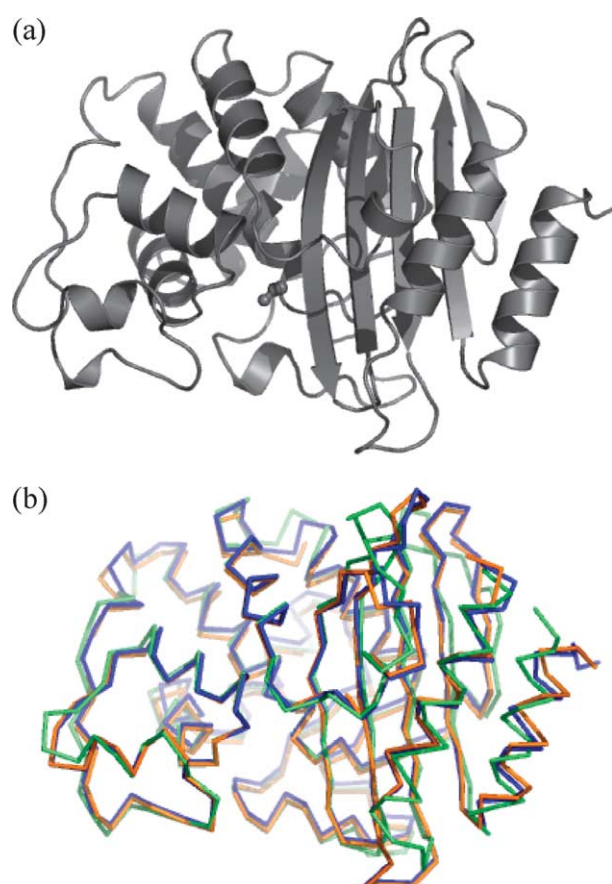[e] Calculated by PROCHECK.[48]

Figure 2. Structures of CTX-M class A β-lactamases. (a) Overall structure of CTX-M-14. The catalytic Ser70 is shown as a stick-and-sphere model. (b) Overlaid backbone structures of CTX-M-14 (blue), TEM-1 (green) and Toho-1 (orange). The three structures are superimposed based on the backbone atoms of residues 70–73, 130–132, 234–236.

C^α atoms between CTX-M-14 and each of CTX-M-9, CTX-M-27, CTX-M-16 are 0.17 Å, 0.32 Å, and 0.17 Å, respectively. Their overall structures resemble those of other class A β-lactamases including TEM-1, SHV-1 and Toho-1 (Figure 2).[4,11,15] They consist of an α/β domain and an α domain, with the active site residing in the interface between these two domains. The C^α rmsd values between CTX-M-14 and each of TEM-1 (pdb ID, 1JWP) and Toho-1 are 2.16 Å and 0.67 Å, respectively. The small overall C^α rmsd difference between CTX-M-14 and Toho-1 reflects the approximately 80% sequence identity between these enzymes.

The ultrahigh-resolution electron density maps for CTX-M-14, CTX-M-27 and CTX-M-9 made it possible to determine accurately the positions of individual atoms (Figure 3). C, N and O atoms can be distinguished from one another based on density volumes; double conformations are observed for multiple protein side-chains in the three structures of 1.2 Å or higher resolutions. Examples include a second conformation for Tyr264 and, in CTX-M-14

and CTX-M-9, for the catalytically critical Lys73 (Figure 3(a) and (b)).

Most backbone hydrogen atoms are visible in $F_o − F_c$ electron-density maps at 1.5σ or higher contour levels, particularly for the 0.98 Å CTX-M-9 structure (Figure 3(c)). Hydrogen atoms for well-ordered side-chains can also be determined at 1.5σ or slightly lower contour levels in the difference maps (Figure 3(d)). Unfortunately, hydrogen atoms cannot be seen for the functional groups of catalytic residues such as Ser70, Lys73 or Glu166.

The high quality of the CTX-M-14, CTX-M-27 and CTX-M-9 crystallographic data enabled us to refine the temperature factors anisotropically and thus to consider coordinated atomic movement in the protein structure. Temperature factors reflect atomic fluctuations in the protein molecules. Whereas only isotropic temperature factors are available for most structures, the high data-to-parameter ratio for ultrahigh-resolution diffraction allows the determination of anisotropic atomic movement. Comparison of the anisotropic temperature factors for CTX-M-14, CTX-M-27 and CTX-M-9 indicates interesting changes in the movement of B3 strand residues (Figure 4). The Asp240Gly substitution in CTX-M-27, which has increased ceftazidimase activity, appears to lead to a concerted fluctuation among the backbone atoms in the B3 strand, an effect detectable even as distant as Gly236 (see Discussion). These concerted fluctuations are apparent both from anisotropy correlation calculations (Table 2) and graphs (Figure 5), and from TLS (translation/libration/screw) analysis (data not shown).

The accuracy of the electron density map also led to the discovery of a spontaneous mutation in the CTX-M-27 clone used in the crystallization studies. Residue 99, originally proline, was identified unambiguously as histidine in the CTX-M-27 structure. We refer to this structure throughout as that of CTX-M-27; notwithstanding the unanticipated extra substitution, this enzyme is isofunctional and isostable with true CTX-M-27. Additionally, a sucrose molecule from the cryoprotectant solution was found to be bound to a pocket formed by residues including 101, 136 and 165. It was modeled in the three atomic-resolution structures with partial occupancy.

Active site

The positions and interactions of most key catalytic residues remain unchanged compared with those of TEM-1 and Toho-1, and we will consequently focus only on features that are new in the CTX-M structures. The atomic-resolution electron density maps allowed us to clearly distinguish two conformations for Lys73 in CTX-M-9 and CTX-M-14 (Figure 6). The two conformations have similar occupancies in both structures (e.g. in CTX-M-9, 0.54 for conformation 1 and 0.46 for conformation 2). In conformation 1, Lys73 hydrogen bonds with the O^γ of Ser70, the $O^{\delta 1}$ of Asn132, and a
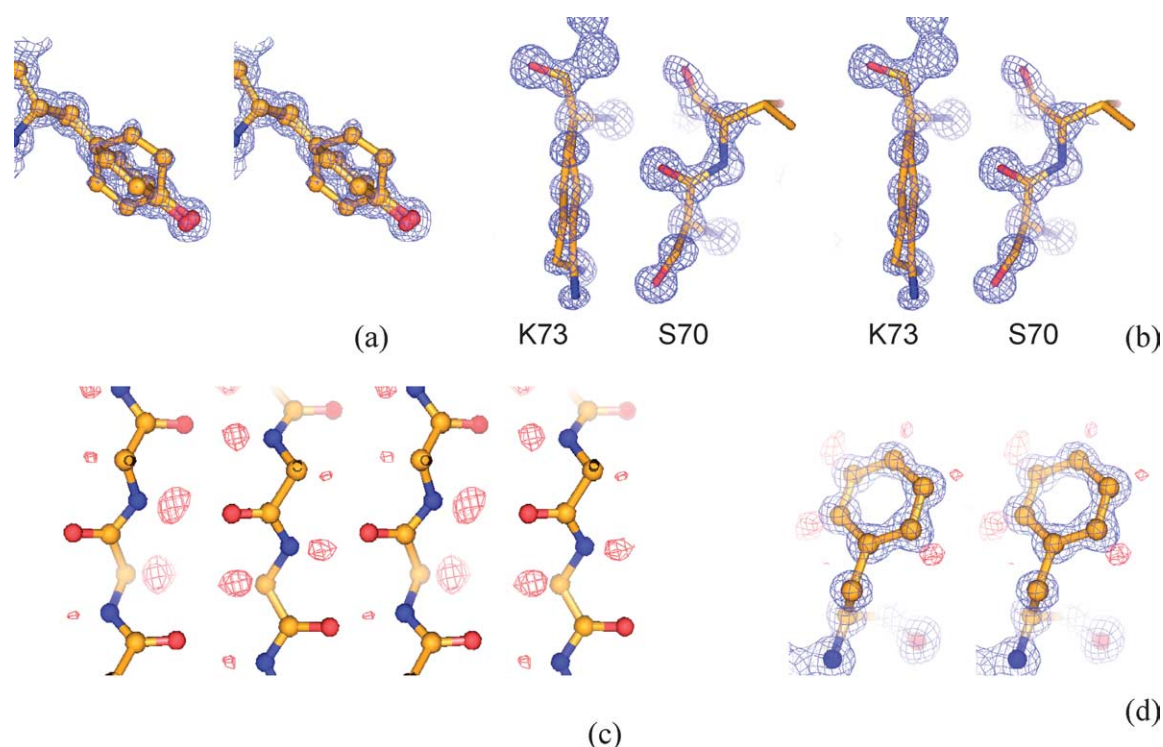
Figure 3. Structural details of the CTX-M-9 atomic resolution electron density map. (a) Stereo view of the double conformations of Tyr264 in a $2F_o - F_c$ map contoured at 1σ (blue). (b) Stereo view of the double conformations observed for the catalytic Lys73 in a $2F_o - F_c$ map contoured at 1.5σ (blue). (c) Stereo view of a β-sheet region showing the main-chain hydrogen atom positions revealed by the hydrogen-omitted $F_o - F_c$ map (red, 2.5σ). (d) Stereo view of Phe265 showing the side-chain hydrogen atom positions indicated by the hydrogen-omitted $F_o - F_c$ map (red, contoured at 1.2σ). The $2F_o - F_c$ map (blue) is contoured at 1.5σ. Carbon, nitrogen and oxygen atoms are colored orange, blue and red, respectively.

water molecule that is also contacted by Glu166 and Ser72 (WAT2), which should not be confused with the catalytic water (WAT1). The WAT2 molecule is absent from the TEM β-lactamase structures in which Ser72 is replaced by phenylalanine. The current orientation of the Glu166 side-chain favors hydrogen bonds with WAT1 and WAT2. Although conformation 1 of Lys73 is within hydrogen bonding distance of Glu166, its geometry is not well suited for classic hydrogen bond formation. Conformation 2 of Lys73 hydrogen bonds with the $O^{\delta 1}$ atom of Asn132, the O^γ atom of Ser70, as well as the O^γ of Ser130. In CTX-M-27 (1.20 Å resolution) and CTX-M-16 (1.74 Å resolution) only conformation 2 is observed.

Activities and stabilities of CTX-M mutants

The four CTX-M enzymes studied here have different activities against cefotaxime and ceftazidime (Table 3).[17,18,24] The mutants differ from one another by two substitutions: Val231Ala and Asp240Gly. Val231 and Asp240 reside at each end of the B3 strand, which contributes key residues to the substrate-binding pocket. The Asp240Gly substitution, distinguishing CTX-M-27 from CTX-M-14, decreases the hydrolytic efficiency against cefotaxime but improves the activity against ceftazidime. The Val231Ala mutation in CTX-M-9, on the

other hand, does not affect the enzyme activity by itself but, in conjuction with Asp240Gly, leads to CTX-M-16, an enzyme significantly more active against both cefotaxime and ceftazidime (Table 3).

We were interested to understand the stability consequences of the substitutions, and specifically to learn whether there was an activity-stability tradeoff. We first had to demonstrate that the enzymes could be denatured in a reversible, two-state manner. Reversibility and equilibrium unfolding were investigated by two criteria: whether CD and fluorescence signals returned to the original, folded values after the protein had been thermally denatured, and whether unfolding curves could be retraced by refolding curves. All melts showed that folded signal returned by more than 98% on cooling after unfolding, and unfolding curves closely resembled refolding curves (Figure 7(a) and (b)). To investigate two-state behavior, we monitored denaturation by CD and fluorescence, often at the same time in a single cuvette. The T_m values and van't Hoff enthalpies by both measurements closely resembled each other, with the van't Hoff enthalpies high in magnitude, consistent with the sharp, cooperative transitions observed. Moreover, T_m values and van't Hoff enthalpies were relatively unaffected by the rate of temperature increase in these denaturations (Table 4). Taken together, these results are consistent with well-behaved, two-state
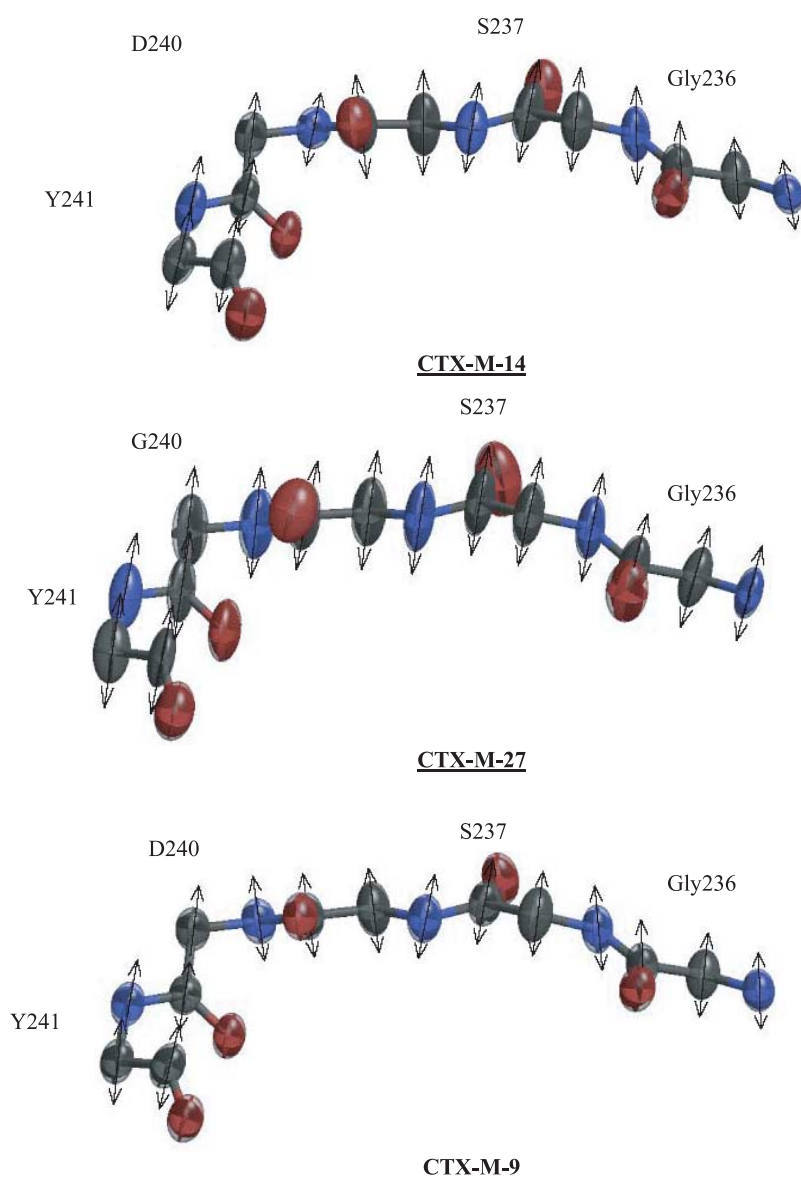
CTX-M-14

CTX-M-27

CTX-M-9

Figure 4. Thermal motions of residues 236–241. (a) CTX-M-14; (b) CTX-M-27; (c) CTX-M-9. The anisotropic displacement parameter (ADP) matrix can be translated into a three-dimensional Gaussian distribution of the electron density. Thermal ellipsoids of the backbone atoms are drawn with 50% probability using Raster3D.[28,44] The major axes of the ellipsoids are indicated by arrows for N (blue), C (gray) and Cα (gray) atoms. Notice that they are better aligned in CTX-M-27 compared with the other two proteins.

reversible thermal denaturation behavior of the CTX-M enzymes, allowing us to analyze thermal denaturation differences thermodynamically.

The Val231Ala substitution in CTX-M-9 caused a 2 deg. C decrease in the protein melting temperature (T_m), or a $\Delta\Delta G$ of -1.1 kcal/mol using the method of Schellman (see Methods), relative to the pseudo-wild-type CTX-M-14, whereas Asp240Gly in CTX-M-27 decreased T_m by 1 deg. C, or a $\Delta\Delta G$ of -0.55 kcal/mol (Figure 7(c)). The effects of these two mutations on enzyme stability were approximately additive, resulting in a 3.3 deg. C difference

Table 2. Comparison of anisotropic temperature factors of the three atomic-resolution structures in the B3 strand region

	Mean anisotropy[a] (backbone atoms)		Anisotropy correlation[b] (residues 236–241 backbone atoms)	
	Residues 236–241	Whole protein	Mean	Range
CTX-M-14 (wt*)	0.343	0.484	1.05	0.99–1.14
CTX-M-27 (D240G)	0.264	0.450	1.09	0.98–1.22
CTX-M-9 (V231A)	0.426	0.535	1.03	0.99–1.07

[a] Anisotropy is defined as the ratio of the smallest and largest eigenvalues of the anisotropic displacement parameter (ADP) matrix.[44] It is reflected in the shape of the thermal ellipsoid. Whereas a sphere has an anistropy of 1, the value decreases as the ellipsoid becomes less spherical.

[b] The normalized correlation coefficient, S_{uij} (U,V), compares the ADP matrices of two atoms (U and V), as defined.[27] The value is greater than 1 when U and V are more similar to each other than to the ADP matrix of an isotropic atom.
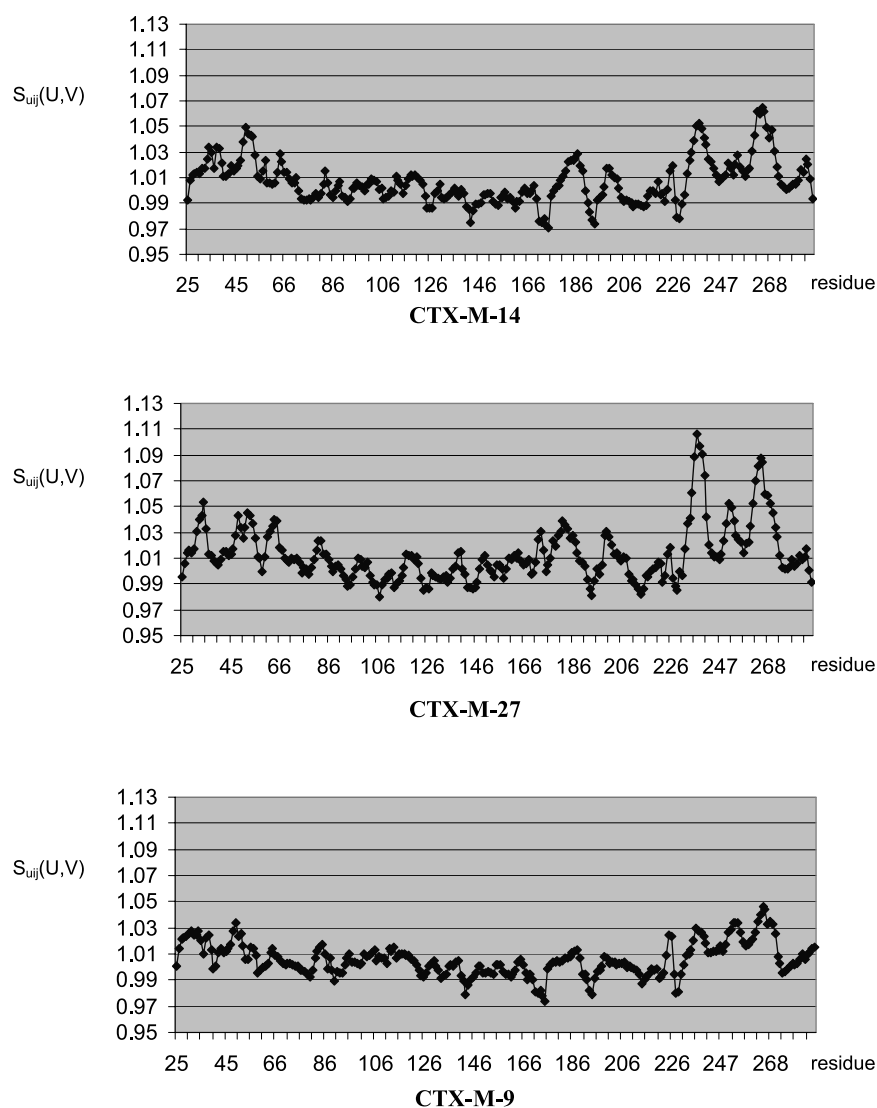
Figure 5. Mean anisotropy correlation of backbone atoms. The normalized correlation coefficient (*Y* axis) is calculated for each pair of backbone atoms and averaged over a sliding window of five amino acid residues. The residue number (*X* axis) represents the first residue in each sliding window. The highest peak in CTX-M-27 corresponds to the region of residues 236–241.
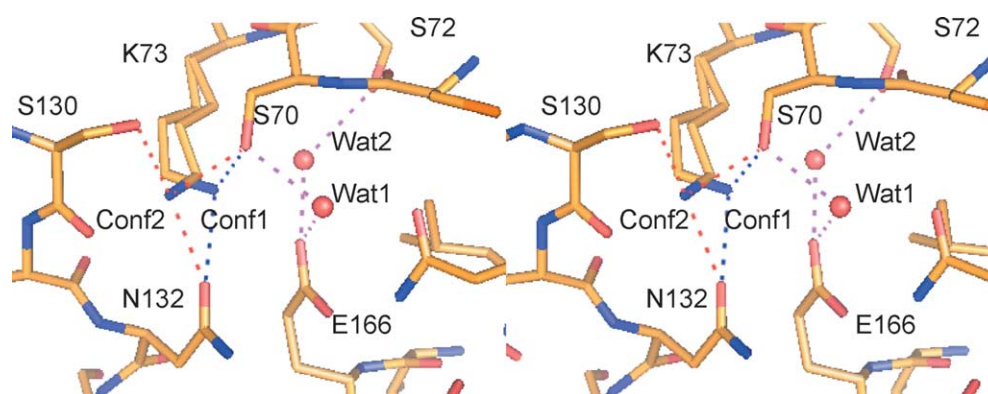

Figure 6. Double conformations of Lys73 in CTX-M-9. (a) Lys73 conformation 1 is within hydrogen bonding distance to Ser70, Asn132 and a water molecule (WAT2). The catalytic water molecule, WAT1, interacts with both Glu166 and Ser70. In addition to Lys73, WAT2 can hydrogen bond with Glu166 and Ser72. (b) Lys73 conformation 2 is able to hydrogen bond with Ser70, Ser130 and Asn132. The interactions involving the catalytic water molecule are also shown.

Table 3. Changes in the T_m, ΔH and kinetic constant values of CTX-M enzymes harboring the amino acid substitutions Val231Ala and Asp240Gly

Enzymes[a]	Circular dichroism			Cephalothin			Cefotaxime			Ceftazidime		
	T_m (°C)	ΔH_{VH} (kcal/mol)	$\Delta\Delta G_u^{b}$ (kcal/mol)	k_{cat} (s^{-1})	K_m (μM)	k_{cat}/K_m (s^{-1} μM^{-1})	k_{cat} (s^{-1})	K_m (μM)	k_{cat}/K_m (s^{-1} μM^{-1})	k_{cat} (s^{-1})	K_m (μM)	k_{cat}/K_m (s^{-1} μM^{-1})
CTX-M-14	50.9±0.3	181±9	–	2700	175	15	415	130	3.2	3	610	0.005
CTX-M-27	49.9±0.2	172±5	−0.55±0.10	232	125	1.8	113	120	0.9	4	191	0.021
ΔCTX-M-27	50.0±0.1	171±6	−0.50±0.05	–	–	–	–	–	–	–	–	–
CTX-M-9	48.9±0.1	133±10	−1.12±0.05	3000	150	20	450	120	3.7	2	600	0.004
CTX-M-16	47.6±0.2	108±3	−1.86±0.10	2800	83	34	1400	150	9.3	15	350	0.043

[a] CTX-M-14, pseudo-wild-type (WT*); CTX-M-27, D240G; ΔCTX-M-27, D240G, P99H (clone used in structural studies, with a spontaneous mutation P99H); CTX-M-9, V231A; CTX-M-16, D240G, V231A.
[b] Determined by the method of Schellman: $\Delta\Delta G_u = \Delta T_m \Delta S_u^{CTX-M-14}$. A negative $\Delta\Delta G_u$ value means a decrease in stability as indicated by a decrease in the T_m value.

between the melting temperatures of CTX-M-16 and CTX-M-14, or a $\Delta\Delta G$ value of −1.86 kcal/mol. Not surprisingly, CTX-M-16, the least stable of these four, yielded crystals that diffracted less well compared with those of the other mutants.

Discussion

These studies reveal both specific and general features of the CTX-M enzymes that explain their extraordinary ESBL activity. A peculiar feature of these enzymes is that, unlike the TEM and SHV ESBLs, but resembling Toho-1, their active site is not enlarged to recognize the bulky third-generation cephalosporins (Figure 1). Instead, ESBL activity appears to depend on particular amino acid complementarities, such as Ser237 and Asn104, which may directly interact with the oxyimino side-chains of third-generation cephalosporins. The enhanced mobility of the B3 strand in the broader spectrum CTX-M-27 may reflect a general mechanism for extending substrate range. The coordinated motion along this strand may represent a type of accommodation that is common among enzymes and is clear here owing to the unusually high resolution of these structures. Correspondingly, the increased mobility of this B3 strand is due to substitutions on either end of it, Asp240Gly and Val231Ala, which diminish the stability of the folded enzyme, consistent with a stability-activity tradeoff in the evolution of resistance enzymes.

Active site

The correlated, anisotropic motion of the B3 strand in CTX-M-27 is the most unexpected and perhaps most generally interesting result to emerge from these structures. CTX-M-27 has four times more activity *versus* ceftazidime, compared to the pseudo-wild-type CTX-M-14. Ceftazidime is a difficult substrate because it is even bulkier than cefotaxime. The way "classical" ESBLs like TEM-64 handle this challenge is by expanding their active site volumes. The accommodation in CTX-M-27 does not appear to increase the volume of its active site in the ground state, but rather increases the range of motion it can undergo. This might increase flexibility, making deformations easier to accommodate larger substrates, or couple thermal energy into the reaction pathway.[25,26]

It is appropriate to consider the experimental thermal anisotropic measurements on which we base this argument. The magnitude of the anisotropic movement is evaluated using an anisotropy parameter that ranges from 0 to 1, with 1 indicating an ideally isotropic atom. Hence, the lower the anisotropy value, the more asymmetric the thermal motion of the atom. The backbone atoms of Gly240 in CTX-M-27, with a mean value of 0.218, display more prominent anisotropic movement than those of Asp240 in CTX-M-14, with a mean value of 0.370 (Table 2 and Figure 4). Similar differences are
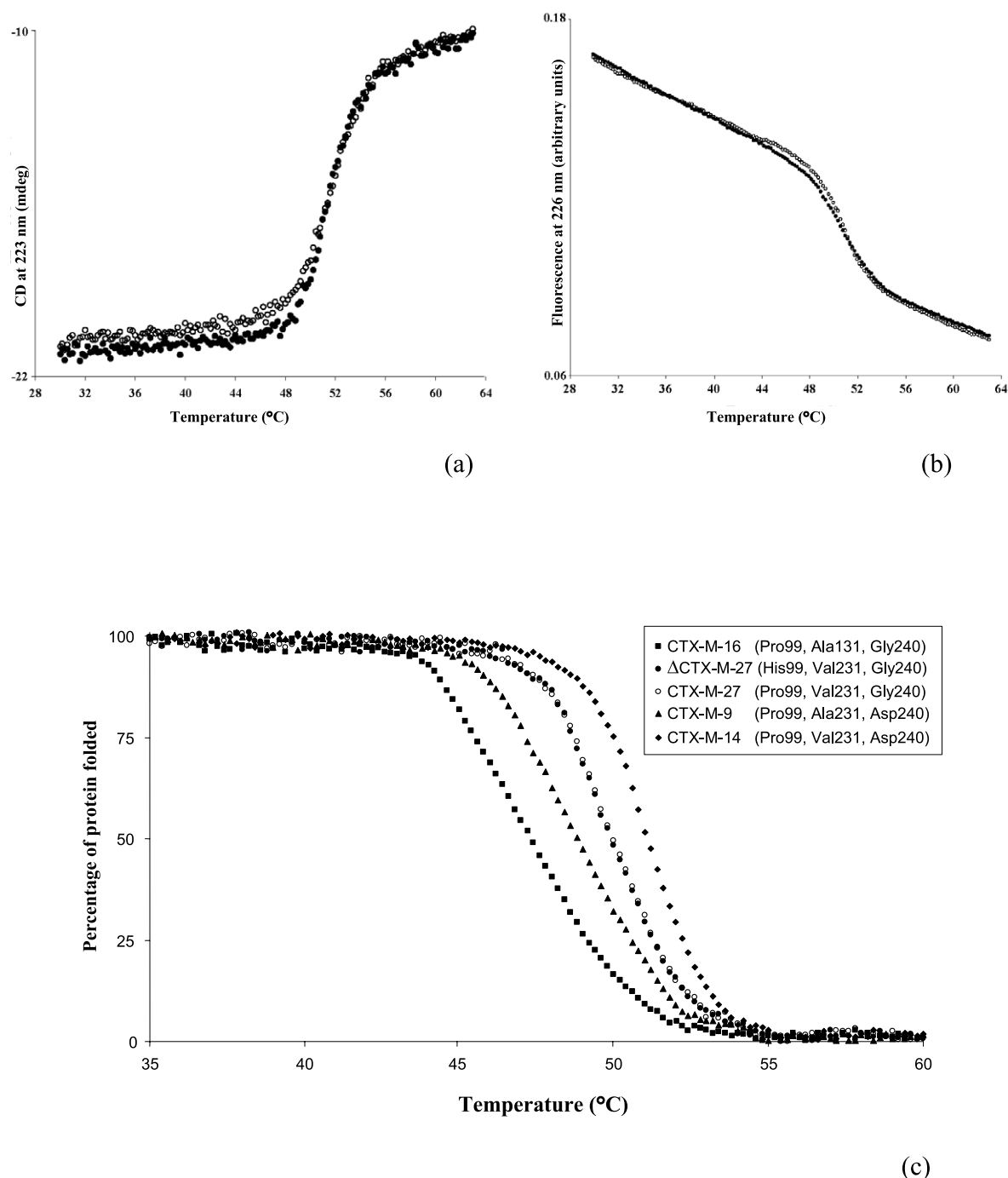
(a)

(b)

(c)

Figure 7. Thermal denaturation of CTX-M mutants. (a) Reversible, two-state thermal denaturation of CTX-M-14 as monitored by far-UV CD at 223 nm. Values are given in Table 4. Filled circles indicate the denaturation (heating) curve and open circles the renaturation (cooling) curve. (b) Reversible, two-state thermal denaturation of CTX-M-14 as monitored by fluorescence at 226 nm. Values are given in Table 4. Filled circles indicate the denaturation step and open circles the renaturation step. (c) Comparison of the thermal denaturation of the four CTX-M mutants monitored by far-UV CD at 223 nm.

observed for main-chain atoms of residues 236–241 in these two proteins, with mean values of 0.264 and 0.343 for CTX-M-27 and CTX-M-14, respectively. Although part of the increased anisotropy magnitude may stem from the different rigid-body movement of the whole protein, the more coordinated movement of the backbone atoms clearly indicates directional changes in the atomic thermal motion in this particular region. The anisotropic movements of the backbone atoms have higher correlation values, quantified by the normalized correlation coefficient, S_{uij} (U,V), as defined in PARVATI and Raster3D.[27,28] An S_{uij} value greater than 1 indicates the anisotropic temperature factors of two atoms are more similar to each other than to an isotropic atom. For CTX-M-27, the mean S_{uij}

Table 4. Reversible, two-state thermal denaturation of CTX-M-14

| Temperature gradients (°C/min) | Circular dichroism | | | Fluorescence | | |
	T_m (°C)	ΔH_{VH} (kcal/mol)	ΔS_u (kcal/mol K)	T_m (°C)	ΔH_{VH} (kcal/mol)	ΔS_u (kcal/mol K)
1	51.0 ± 0.3	178 ± 11	0.55 ± 0.04	50.6 ± 0.3	183 ± 11	0.56 ± 0.04
2	50.9 ± 0.3	181 ± 9	0.56 ± 0.03	50.5 ± 0.3	202 ± 12	0.61 ± 0.05
3	51.0 ± 0.1	187 ± 8	0.58 ± 0.03	50.7 ± 0.1	205 ± 6	0.63 ± 0.02

value is 1.09 for the backbone atoms of residues 236–241, while that of CTX-M-14 is 1.05. Such significant alterations are not observed in other parts of the protein between CTX-M-27 and CTX-M-14, where the mean S_{uij} value varies no more than 0.02 between the two proteins (Figure 5). The correlated motion is readily noticeable in the thermal ellipsoids drawn to visualize these anisotropic movements (Figure 4). For Gly236 atoms, for instance, the directions of their thermal motions are altered in CTX-M-27 so that they are more correlated with the rest of the backbone atoms in this region.

The anisotropy changes may reflect not only the increased flexibility of a Gly relative to an Asp in WT*, but also the loss of interactions between Asp240 and surrounding residues, such as Gln270 and Asn170, the latter in the Ω loop region. The Asp240Gly substitution makes it easier for the B3 strand to move in a more orchestrated manner. It was speculated that the flexibility of the B3 strand in ESBLs can assist the binding of third-generation cephalosporins.[19] CTX-M-type enzymes have glycine residues at positions 232, 236 and 238, with Gly232 present only in ESBLs. Our results support this hypothesis. Whereas no effect on anisotropy is observed by the Val231Ala substitution in CTX-M-9, this residue is on the other end of the B3 strand and it may be that, when the two substitutions occur together, in CTX-M-16, the movement of the B3 strand is further enhanced. Unfortunately, the CTX-M-16 crystal did not diffract to a high enough resolution to investigate this point directly. Nevertheless, the non-additive increase in activity observed among D240G (CTX-M-27), V231A (CTX-M-9) and D240G/V231A (CTX-M-16) is consistent with this hypothesis.

There are indications that the increased mobility of the B3 strand may have echoes in other regions of the structure. In Toho-1, for instance, it has been proposed that the cefotaximase and ceftazidimase activities are partly explained by increased flexibility of the Ω loop and of the loop between B3 and B4, both part of the binding pocket.[15,19,20] Consistent with this view, there are fewer interactions between the Ω loop and the α/β domain of the CTX-M structures determined here, compared with TEM and SHV enzymes. Some of the hydrogen bonds connecting the N and C termini of the Ω loop are also lost in the CTX-M-like enzymes, such as the one between Thr160 (replaced by a phenylalanine) and Thr/Ser181 in non-ESBL β-lactamases.

The structural flexibility of the enzyme can be visualized in the multiple conformations of protein side-chains and, in some cases, the backbone. Although our density maps did not reveal any prominent alternative conformations for side-chains inside the Ω loop and B3 strand region, side-chain movement is apparent in the protein core, in areas close to the ends of the Ω loop and helix H2, which harbors Lys73. Double conformations were modeled for Met75, Met186 and Tyr264, which are close to one another in tertiary structure. No alternative conformation is observed for Tyr264 in the ultrahigh-resolution structure of the non-ESBL TEM-1 structure (0.85 Å),[7] which shares a high level of sequence similarity with CTX-M-type enzymes in these regions. The second conformation of Met186 allows the placement of a water molecule inside the protein to interact with the backbone N atom of Met75, further highlighting the structural flexibility of this region. Met186 also has double conformations in the 0.85 Å TEM-1 structure but there is significantly less variation between the two conformations compared with that in our structures. Met75 is replaced in TEM-1 by a smaller residue Leu75, which exhibits two conformations as well.

Substrate recognition and catalysis

Whereas protein flexibility partly accounts for extended substrate range in the CTX-M family, new interactions can also be formed between these enzymes and substrates compared with TEM and SHV ESBLs. Two such residues are Ser237 and Asn104, both part of the substrate-binding pocket. Residues 237 and 104 are alanine and glutamate, respectively, in non-ESBL TEM and SHV enzymes. The Ala237Thr substitution in TEM enzymes improved their cephalosporinase activities,[29–31] and the Ser237Ala substitution decreased hydrolytic efficiency against oxyimino-cephalosporins in CTX-M-4 and *Proteus vulgaris* K1 β-lactamase, both ESBLs.[32,33] Ser237 and Asn104 interact with the carboxylate group of cefotaxime and the carbonyl group of the acylamide side-chain, respectively, in the acyl intermediate structure of Toho-1.[20] The importance of these two residues for CTX-M-like enzymes make them suitable targets for inhibitor development against this new group of ESBLs.

Whereas the identities and locations of the key active site residues are conserved amongst ESBL and non-ESBL class A β-lactamases, Lys73 in the

CTX-M family of enzymes shows unusual, and mechanistically intriguing, flexibility. Unlike the apo structures of TEM and SHV enzymes, Lys73 adopts two conformations in two of the three ultrahigh-resolution CTX-M structures determined here, as well as in the Toho-1 structure. In the first conformation, shared with the other class A enzymes, this lysine residue hydrogen bonds with Ser70. In the second conformation, clearly visible at ultrahigh resolution, the terminal N$^{\zeta}$ shifts 1.5 Å to hydrogen bond with Ser130 (Figure 6). What makes this change intriguing is that Lys73 is thought to activate the hydrolytic Ser70 for attack on the substrate, either directly or indirectly, in the initial hydrolytic step.[6,34–36] Subsequently, Lys73 is proposed to activate Ser130, which is thought to act as a general acid promoting departure of the β-lactam nitrogen atom on the way to the formation of the enzyme-substrate acyl-adduct.[36,37] The two positions of Lys73 in CTX-M-9 and CTX-M-14 are consistent with it shuttling between subsequent steps along the reaction coordinate. It may be that these conformations are similar enough in energy to be accessible in most apo class A β-lactamases, though they are not seen in TEM-1, SHV-1, or even CTX-M-27 and CTX-M-16. In CTX-M-9, CTX-M-14 the energy difference is so small that both catalytically important conformations are visible at ultrahigh resolution.

Activity and stability tradeoff

The enlargement of the active site cleft in ESBL TEM and SHV mutants is accompanied by a loss of protein stability, due to the loss of intra-molecular interactions or to the structural strain sustained to avoid steric clash.[4,10,12] Although the two substitutions (Val231Ala and Asp240Gly) in CTX-M enzymes did not alter the active site configuration, both decreased protein stability, presumably because of loss of favorable packing and polar interactions (Table 3). Comparing CTX-M-14 (WT*) and CTX-M-9 (V231A) structures suggests that the Val231Ala substitution results in a small cavity in the protein side-chain packing, causing a small movement in both the backbone and side-chain conformations of nearby residues to partially compensate for this local defect (Figure 8). The buried interface between the Val231 side-chain and surrounding residues is 238 Å^2 while that for Ala231 is 151 Å^2. This loss of van der Waals interactions and buried hydrophobic surface contributes to the stability decrease of 1.1 kcal/mol. On the other end of the B3 strand, the Asp240Gly substitution breaks several van der Waals and hydrogen bond interactions with surrounding residues and ordered water molecules, leading to a 0.55 kcal/mol loss in stability.

This returns us to what is perhaps the most striking and generally interesting feature to emerge from this study, the increased coordinated movement along the catalytically critical B3 strand of the active site. This strand contributes two residues
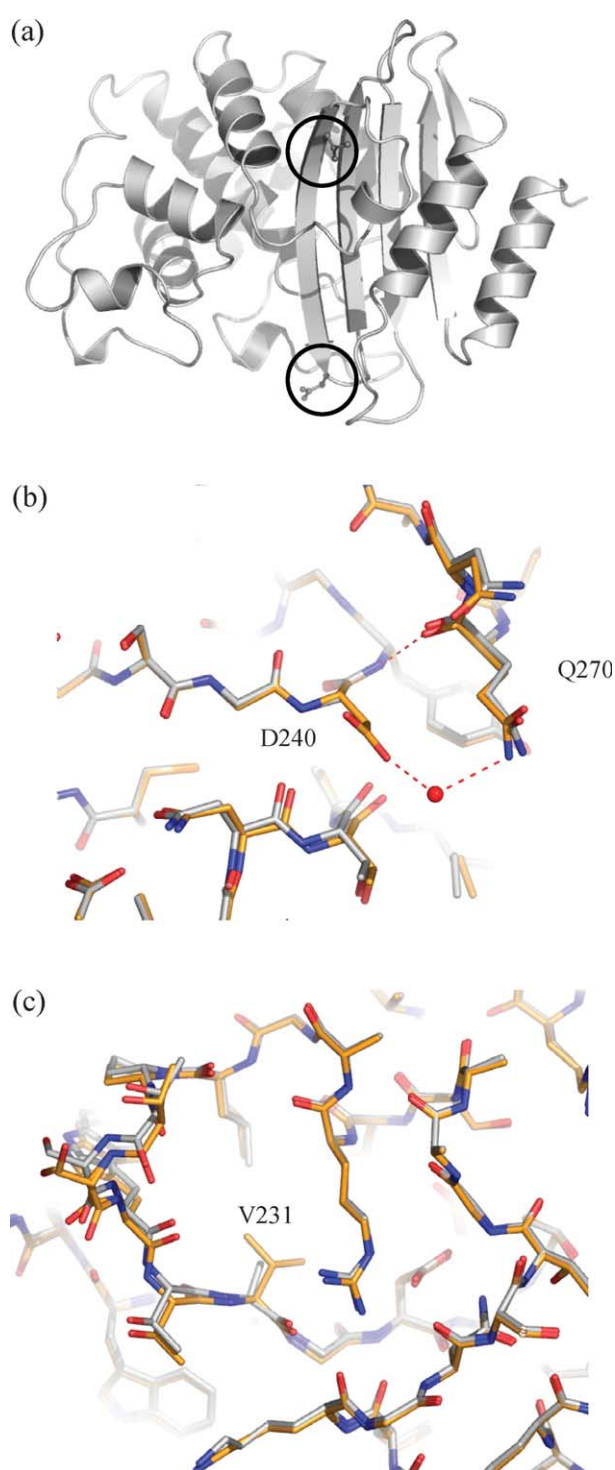

Figure 8. The effects of Asp240Gly and Val231Ala mutations. (a) Asp240 and Val231, shown as stick-and-sphere models and circled, are positioned at the two ends of the B3 strand. (b) Comparison of CTX-M-14 and CTX-M-27 (white) in the region of the Asp240Gly substitution. The side-chain of Asp240 and the main chain of Tyr241 are involved in indirect and direct intra-molecular hydrogen bonding, respectively. (c) Comparison of CTX-M-14 and CTX-M-9 (white) in the region of the Val231Ala substitution.

essential to catalytic activity, Lys234 and the main chain of Ser237, which forms part of the enzyme's "oxyanion" hole,[38,39] and several substrate-recognition residues. In the CTX-M ESBLs, unlike those of TEM and SHV, increased activity against the bulky third-generation cephalosporins, especially ceftazidime, appears to come not from gross enlargement of the active site, but from increased flexibility of this strand, and possibly other regions. This increased flexibility is correlated with higher ceftazidimase activity and lower stability. Structurally, this can be reconciled with the substitutions Asp240Gly and Val231Ala, which occur at either end of the B3 strand. These substitutions create structural defects, apparently loosening the strand in a coordinated manner, at the cost of internal stability. Although the specific origins of the resulting stability-activity tradeoff are peculiar to this enzyme, the mechanism of increased flexibility and diminished stability may be a general aspect of this relationship, which has previously been described in terms of the time-averaged structure of enzymes.[21–23] Here, a coordinated motion aspect of the relationship, long hypothesized for enzymes, is apparent at ultrahigh resolution.[25,26]

Methods

Protein purification

The CTX-M-encoding genes were cloned into a modified plasmid vector pET-9a, as described.[40] *Escherichia coli* BL21(DE3) (Novagen) transformed with the plasmid pET-bla$_{CTX-M}$ was cultured in 2×YT broth containing cefotaxime at 2 μg/ml at 37 °C for five hours. Overexpression of the CTX-M-encoding genes was induced with 0.1 mM isopropyl β-D-thiogalactopyrano-side overnight at 30 °C. Cells were harvested by centrifugation (10,000 *g* for ten minutes at 4 °C) and then disrupted by ultrasonic treatment (four times for 30 seconds, each time at 20 W). The extract was clarified by centrifugation at 48,000 *g* for 60 minutes at 4 °C. After addition of 2 μg of DNase I (Roche), the supernatant was dialyzed overnight against 20 mM Mes–NaOH (pH 6.0). The purification was carried out by ion-exchange chromatography on a fast-flow CM column (Amersham Pharmacia Biotech) in 20 mM Mes buffer (pH 6.0) and eluted with a linear 0–0.15 M NaCl gradient. The enzyme was more than 95% homogeneous as judged by Coomassie blue staining after SDS-PAGE. The purified protein was dialyzed against 5 mM Tris–HCl buffer (pH 7.0) and concentrated to 20 mg/ml for crystallization.

Crystallization and structure determination

CTX-M crystals were grown in hanging drops over a well solution of 1.6 M (NH$_4$)$_2$SO$_4$ and 0.1 M sodium acetate (pH 4.5): 2 μl of 10–15 mg/ml of protein and 2 μl of well solution was mixed and the drop was seeded with microcrystals of CTX-M-27 previously grown under the same conditions. Crystals reached a size of 0.1 mm× 0.1 mm×0.2 mm within two or three days. The space group was $P2_12_12_1$ with cell dimensions of approximately 41 Å, 62 Å, 87 Å, varying slightly among crystals of different proteins. Data were collected at ALS beamline 8.3.1 and processed with the HKL suite.[41] An initial structure was obtained by molecular replacement program EPMR using the Toho-1 apo structure as a search model. Three atomic-resolution structures, CTX-M-14, CTX-M-9 and CTX-M-27, were refined using SHELX97,[42] whereas CTX-M-16 was refined by CNS1.1.[43] For the first three structures, the models were refined using aniso-tropic displacement parameters (ADPs) with standard DELU (rigid-bond restraint), SIMU (restraint for spatially adjacent atoms) and ISOR (isotropic restraint for individual atoms). These values were later adjusted using the program PARVATI.[44] The rmsd values between structures were calculated using the program Chimera.[45] The buried surface areas involving residue 231 were calculated by CNS1.1. Anisotropy analysis was carried out using Parvati, Raster3D, and a program kindly provided by Dr Ethan Merritt to calculate $S_{uij}(U,V)$ between atom pairs.

Protein stability

Protein unfolding and refolding was monitored by circular dichroism (CD) and fluorescence in a Jasco J-715 spectropolarimeter with a Peltier-effect temperature controller and an in-cell temperature monitor. The enzyme was denatured in 38% (v/v) ethylene glycol, 50 mM potassium phosphate (pH 7.0), 200 mM KCl and monitored by far-UV (223 nm) CD and by integrated fluorescence emissions above 300 nm, exciting at 226 nm. We were able to measure fluorescent melts concurrently with CD melts by monitoring the CD at 226 nm and using this wavelength as the excitation wavelength for the fluorescence; this was useful for analyzing two-state behavior. The denaturation was reversible for all proteins and apparently two-state. The melting temperature and van't Hoff enthalpy of unfolding were calculated by the two-state thermodynamics fitting program EXAM.[46] The free energy of unfolding relative to CTX-M-14 was determined by the method of Schellman: $\Delta\Delta G_u = \Delta T_m \Delta S_u^{CTX-M-14}$.[47]

Data deposition

The coordinates and structural factors have been deposited in the RCSB Protein Data Bank: CTX-M-14 (1YLT), CTX-M-9 (1YLJ), CTX-M-27 (1YLP), and CTX-M-16 (1YLW).

References

1. Bradford, P. A. (2001). Extended-spectrum beta-lactamases in the 21st century: characterization, epidemiology, and detection of this important resistance threat. *Clin. Microbiol. Rev.* **14**, 933–951.

2. Paterson, D. L., Ko, W. C., Von Gottberg, A., Mohapatra, S., Casellas, J. M., Goossens, H. *et al.* (2004). Antibiotic therapy for *Klebsiella pneumoniae* bacteremia: implications of production of extended-spectrum beta-lactamases. *Clin. Infect Dis.* **39**, 31–37.

3. Matagne, A. & Frère, J. M. (1995). Contribution of mutant analysis to the understanding of enzyme catalysis: the case of class A beta-lactamases. *Biochim. Biophys. Acta*, **1246**, 109–127.

4. Wang, X., Minasov, G. & Shoichet, B. K. (2002). Evolution of an antibiotic resistance enzyme constrained by stability and activity trade-offs. *J. Mol. Biol.* **320**, 85–95.

5. Wang, X., Minasov, G. & Shoichet, B. K. (2002). Non-covalent interaction energies in covalent complexes: TEM-1 beta-lactamase and beta-lactams. *Proteins: Struct. Funct. Genet.* **47**, 86–96.

6. Strynadka, N. C., Adachi, H., Jensen, S. E., Johns, K., Sielecki, A., Betzel, C. *et al.* (1992). Molecular structure of the acyl-enzyme intermediate in beta-lactam hydrolysis at 1.7 Å resolution. *Nature*, **359**, 700–705.

7. Minasov, G., Wang, X. & Shoichet, B. K. (2002). An ultrahigh resolution structure of TEM-1 beta-lactamase suggests a role for Glu166 as the general base in acylation. *J. Am. Chem. Soc.* **124**, 5333–5340.

8. Jelsch, C., Mourey, L., Masson, J. M. & Samama, J. P. (1993). Crystal structure of *Escherichia coli* TEM1 beta-lactamase at 1.8 Å resolution. *Proteins: Struct. Funct. Genet.* **16**, 364–383.

9. Jelsch, C., Lenfant, F., Masson, J. M. & Samama, J. P. (1992). Beta-lactamase TEM-1 of *E. coli*. Crystal structure determination at 2.5 Å resolution. *FEBS Letters*, **299**, 135–142.

10. Orencia, M. C., Yoon, J. S., Ness, J. E., Stemmer, W. P. & Stevens, R. C. (2001). Predicting the emergence of antibiotic resistance by directed evolution and structural analysis. *Nature Struct. Biol.* **8**, 238–242.

11. Kuzin, A. P., Nukaga, M., Nukaga, Y., Hujer, A. M., Bonomo, R. A. & Knox, J. R. (1999). Structure of the SHV-1 beta-lactamase. *Biochemistry*, **38**, 5720–5727.

12. Nukaga, M., Mayama, K., Hujer, A. M., Bonomo, R. A. & Knox, J. R. (2003). Ultrahigh resolution structure of a class A beta-lactamase: on the mechanism and specificity of the extended-spectrum SHV-2 enzyme. *J. Mol. Biol.* **328**, 289–301.

13. Bonnet, R. (2004). Growing group of extended-spectrum beta-lactamases: the CTX-M enzymes. *Antimicrob. Agents Chemother.* **48**, 1–14.

14. Ishii, Y., Ohno, A., Taguchi, H., Imajo, S., Ishiguro, M. & Matsuzawa, H. (1995). Cloning and sequence of the gene encoding a cefotaxime-hydrolyzing class A beta-lactamase isolated from *Escherichia coli*. *Antimicrob. Agents Chemother.* **39**, 2269–2275.

15. Ibuka, A. S., Ishii, Y., Galleni, M., Ishiguro, M., Yamaguchi, K., Frère, J. M. *et al.* (2003). Crystal structure of extended-spectrum beta-lactamase

16. Poirel, L., Gniadkowski, M. & Nordmann, P. (2002). Biochemical analysis of the ceftazidime-hydrolysing extended-spectrum beta-lactamase CTX-M-15 and of its structurally related beta-lactamase CTX-M-3. *J. Antimicrob. Chemother.* **50**, 1031–1034.

17. Bonnet, R., Dutour, C., Sampaio, J. L., Chanal, C., Sirot, D., Labia, R. *et al.* (2001). Novel cefotaximase (CTX-M-16) with increased catalytic efficiency due to substitution Asp-240→Gly. *Antimicrob. Agents Chemother.* **45**, 2269–2275.

18. Bonnet, R., Recule, C., Baraduc, R., Chanal, C., Sirot, D., De Champs, C. & Sirot, J. (2003). Effect of D240G substitution in a novel ESBL CTX-M-27. *J. Antimicrob. Chemother.* **52**, 29–35.

19. Ibuka, A., Taguchi, A., Ishiguro, M., Fushinobu, S., Ishii, Y., Kamitori, S. *et al.* (1999). Crystal structure of the E166A mutant of extended-spectrum beta-lactamase Toho-1 at 1.8 Å resolution. *J. Mol. Biol.* **285**, 2079–2087.

20. Shimamura, T., Ibuka, A., Fushinobu, S., Wakagi, T., Ishiguro, M., Ishii, Y. & Matsuzawa, H. (2002). Acyl-intermediate structures of the extended-spectrum class A beta-lactamase, Toho-1, in complex with cefotaxime, cephalothin, and benzylpenicillin. *J. Biol. Chem.* **277**, 46601–46608.

21. Shoichet, B. K., Baase, W. A., Kuroki, R. & Matthews, B. W. (1995). A relationship between protein stability and protein function. *Proc. Natl Acad. Sci. USA*, **92**, 452–456.

22. Schreiber, G., Buckle, A. M. & Fersht, A. R. (1994). Stability and function: two constraints in the evolution of barstar and other proteins. *Structure*, **2**, 945–951.

23. Beadle, B. M. & Shoichet, B. K. (2002). Structural bases of stability-function tradeoffs in enzymes. *J. Mol. Biol.* **321**, 285–296.

24. Dutour, C., Bonnet, R., Marchandin, H., Boyer, M., Chanal, C., Sirot, D. & Sirot, J. (2002). CTX-M-1, CTX-M-3, and CTX-M-14 beta-lactamases from Enterobacteriaceae isolated in France. *Antimicrob. Agents Chemother.* **46**, 534–537.

25. Rod, T. H., Radkiewicz, J. L. & Brooks, C. L., III (2003). Correlated motion and the effect of distal mutations in dihydrofolate reductase. *Proc. Natl Acad. Sci. USA*, **100**, 6980–6985 (Epub, May 19).

26. Schnell, J. R., Dyson, H. J. & Wright, P. E. (2004). Structure, dynamics, and catalytic function of dihydrofolate reductase. *Annu. Rev. Biophys. Biomol. Struct.* **33**, 119–140.

27. Merritt, E. A. (1999). Comparing anisotropic displacement parameters in protein structures. *Acta Crystallog. sect. D*, **55**, 1997–2004.

28. Merritt, E. A. & Bacon, D. J. (1997). Raster3D: photorealistic molecular graphics. *Methods Enzymol.* **277**, 505–524.

29. Knox, J. R. (1995). Extended-spectrum and inhibitor-resistant TEM-type beta-lactamases: mutations, specificity, and three-dimensional structure. *Antimicrob. Agents Chemother.* **39**, 2593–2601.

30. Giakkoupi, P., Hujer, A. M., Miriagou, V., Tzelepi, E., Bonomo, R. A. & Tzouvelekis, L. S. (2001). Substitution of Thr for Ala-237 in TEM-17, TEM-12 and TEM-26: alterations in beta-lactam resistance conferred on *Escherichia coli*. *FEMS Microbiol. Letters*, **201**, 37–40.

31. Blazquez, J., Negri, M. C., Morosini, M. I., Gomez-

Gomez, J. M. & Baquero, F. (1998). A237T as a modulating mutation in naturally occurring extended-spectrum TEM-type beta-lactamases. *Antimicrob. Agents Chemother.* **42**, 1042–1044.

32. Gazouli, M., Tzelepi, E., Sidorenko, S. V. & Tzouvelekis, L. S. (1998). Sequence of the gene encoding a plasmid-mediated cefotaxime-hydrolyzing class A beta-lactamase (CTX-M-4): involvement of serine 237 in cephalosporin hydrolysis. *Antimicrob. Agents Chemother.* **42**, 1259–1262.

33. Tamaki, M., Nukaga, M. & Sawai, T. (1994). Replacement of serine 237 in class A beta-lactamase of *Proteus vulgaris* modifies its unique substrate specificity. *Biochemistry*, **33**, 10200–10206.

34. Gibson, R. M., Christensen, H. & Waley, S. G. (1990). Site-directed mutagenesis of beta-lactamase I. Single and double mutants of Glu-166 and Lys-73. *Biochem. J.* **272**, 613–619.

35. Strynadka, N. C., Jensen, S. E., Alzari, P. M. & James, M. N. (1996). A potent new mode of beta-lactamase inhibition revealed by the 1.7 Å X-ray crystallographic structure of the TEM-1-BLIP complex. *Nature Struct. Biol.* **3**, 290–297.

36. Matagne, A., Lamotte-Brasseur, J. & Frère, J. M. (1998). Catalytic properties of class A beta-lactamases: efficiency and diversity. *Biochem. J.* **330**, 581–598.

37. Imtiaz, U., Billings, E. M., Knox, J. R. & Mobashery, S. (1994). A structure-based analysis of the inhibition of class A beta-lactamases by sulbactam. *Biochemistry*, **33**, 5728–5738.

38. Murphy, B. P. & Pratt, R. F. (1988). Evidence for an oxyanion hole in serine beta-lactamases and DD-peptidases. *Biochem. J.* **256**, 669–672.

39. Curley, K. & Pratt, R. F. (2000). The oxyanion hole in serine beta-lactamase catalysis: interactions of thiono substrates with the active site. *Bioorg. Chem.* **28**, 338–356.

40. Bonnet, R., Sampaio, J. L., Chanal, C., Sirot, D., De Champs, C., Viallard, J. L. *et al*. (2000). A novel class A extended-spectrum beta-lactamase (BES-1) in *Serratia marcescens* isolated in Brazil. *Antimicrob. Agents Chemother.* **44**, 3061–3068.

41. Otwinowski, Z. & Minor, W. (1997). Processing of X-ray diffraction data collected in oscillation mode. *Methods Enzymol.* **276**, 307–326.

42. Sheldrick, G. M. & Schneider, T. R. (1997). SHELXL: high-resolution refinement. *Methods Enzymol.* **277**, 319–343.

43. Brünger, A. T., Adams, P. D., Clore, G. M., DeLano, W. L., Gros, P., Grosse-Kunstleve, R. W. *et al*. (1998). Crystallography & NMR system: a new software suite for macromolecular structure determination. *Acta Crystallog. sect. D*, **54**, 905–921.

44. Merritt, E. A. (1999). Expanding the model: anisotropic displacement parameters in protein structure refinement. *Acta Crystallog. sect. D*, **55**, 1109–1117.

45. Pettersen, E. F., Goddard, T. D., Huang, C. C., Couch, G. S., Greenblatt, D. M., Meng, E. C. & Ferrin, T. E. (2004). UCSF Chimera–a visualization system for exploratory research and analysis. *J. Comput. Chem.* **25**, 1605–1612.

46. Kirchhoff, W. (1993). EXAM: a two-state thermodynamic analysis program. *National Institute of Standards and Technology Technical Note 1401*, National Institute of Standards and Technology, US Department of Commerce Technology Administration, Washington, DC.

47. Becktel, W. J. & Schellman, J. A. (1987). Protein stability curves. *Biopolymers*, **26**, 1859–1877.

48. Laskowski, R. A., MacArthur, M. W., Moss, D. S. & Thornton, J. M. (1993). PROCHECK: a program to check the stereochemical quality of protein structures. *J. Appl. Crystallog.* **26**, 283–291.